Hard pion bremsstrahlung in the Coulomb region

Göran Fäldt* and Ulla Tengblad†
Department of Nuclear and Particle Physics, Uppsala University, Box 535, S-751 21 Uppsala, Sweden
(Received 1 September 2007; published 20 December 2007)

Hard high-energy pion-nucleus bremsstrahlung, $\pi^- + A \to \pi^- + \gamma + A$, is studied in the Coulomb region, i.e., the small-angle region where the nuclear scattering is dominated by the Coulomb interaction. Special attention is focussed on the possibility of measuring the pion polarizability in such reactions. We study the sensitivity to the structure of the underlying pion-Compton amplitude through a model with σ, ρ, and a_1 exchanges. It is found that the effective energy in the virtual pion-Compton scattering is often so large that the threshold approximation does not apply.

DOI: 10.1103/PhysRevC.76.064607 PACS number(s): 13.40.−f, 24.10.Ht, 25.80.Hp

I. INTRODUCTION

High-energy pionic bremsstrahlung, i.e., the coherent nuclear reaction

$$\pi^- + A \to \pi^- + \gamma + A$$

can proceed through a one-photon exchange. In fact, at small momentum transfers to the nucleus A, the reaction is dominated by the virtual pion-Compton reaction $\gamma + \pi^- \to \gamma + \pi^-$. A long time ago it was suggested [1,2], that by studying pionic bremsstrahlung important information on the pion-Compton amplitude could be extracted. Of particular interest is the pion electric and magnetic polarizabilities, which are low-energy parameters that have been calculated in chiral-Lagrangian theory [3]. A bremsstrahlung experiment aiming at measuring the polarizabilities has been performed [4], and reasonable values of these parameters were extracted. The pion polarizabilities can also be determined in other reactions, such as pion photoproduction [5].

At low energies the pion-Compton amplitude can be regarded as a sum of two contributions, a structure-independent Born term, and a structure-dependent term fixed by the pion polarizabilities. At higher energies the situation is more complex. Therefore, we have chosen to model the pion-Compton amplitude as a sum of the Born amplitudes, and the amplitudes generated by the σ, ρ, and a_1 exchanges. This model should be fairly reliable also in the early GeV region.

In a previous paper [6] we developed a Glauber model for pion-nucleus bremsstrahlung. Such a model includes nuclear scattering and is also valid for momentum transfers outside the Coulomb region of small momentum transfers. For the pion-Compton amplitude only the Born terms and the polarizabilities were retained. However, it was pointed out that in applications one quickly comes into a region of high energies in the virtual pion-Compton scattering. In the present paper we direct our interest at exactly this energy dependence. The meson-exchange model is then the reasonable starting point. Furthermore, we consider only the small-angle region where it is sufficient to retain the Coulomb interaction alone, and neglect all nuclear interactions.

II. PION-COMPTON SCATTERING

The primary mechanism responsible for pion-nucleus bremsstrahlung in the Coulomb region is pion-Compton scattering, involving a virtual photon exchange between the pion and the nucleus. In our previous investigation [6] we used the low-energy approximation of the pion-Compton amplitude, as parametrized by the pion polarizabilities. Now, we want to go beyond this approximation, and investigate, in a model, the limits of the low-energy approximation in actual applications. We shall assume that, in addition to the Born terms, the pion-Compton amplitude receives contributions also from the σ, ρ and a_1 exchange diagrams.

The Compton amplitude is written as

$$\mathcal{M}(\gamma(q_1)\pi^-(p_1) \to \gamma(q_2)\pi^-(p_2)) = \mathcal{M}_{\mu\nu}\epsilon_1^\mu(q_1)\epsilon_2^\nu(q_2).$$

Gauge invariance requires that, for real as well as virtual photons with $q^2 \neq 0$, the Compton tensor satisfies

$$\mathcal{M}_{\mu\nu}q_1^\mu = \mathcal{M}_{\mu\nu}q_2^\nu = 0.$$

The Compton tensor $\mathcal{M}_{\mu\nu}$ is conveniently decomposed as

$$\mathcal{M}_{\mu\nu} = ie^2\left[A(s,t)\mathcal{A}_{\mu\nu} + B(s,t)\mathcal{B}_{\mu\nu}\right], \tag{1}$$

with the gauge-invariant tensors $\mathcal{A}_{\mu\nu}$ and $\mathcal{B}_{\mu\nu}$ defined as

$$\mathcal{A}_{\mu\nu} = 2g_{\mu\nu} - \frac{(2p_2+q_2)_\nu(2p_1+q_1)_\mu}{s-m_\pi^2} - \frac{(2p_1-q_2)_\nu(2p_2-q_1)_\mu}{u-m_\pi^2}, \tag{2}$$

$$\mathcal{B}_{\mu\nu} = q_1\cdot q_2 g_{\mu\nu} - q_{2\mu}q_{1\nu}, \tag{3}$$

and the Mandelstam kinematic variables by

$$\begin{aligned} s &= (p_2+q_2)^2, \\ t &= (p_1-p_2)^2, \\ u &= (p_1-q_2)^2. \end{aligned} \tag{4}$$

For pions there are three Born amplitudes described by the Feynman diagrams of Fig. 1. In the decomposition of Eq. (1)

*goran.faldt@tsl.uu.se
†ulla.tengblad@tsl.uu.se

FIG. 1. Born diagrams for pion-Compton scattering.

the invariant functions $A(s,t)$ and $B(s,t)$ are

$$A(s,t) = 1, \tag{5}$$

$$B(s,t) = 0. \tag{6}$$

In our previous study we went beyond the Born approximation, adding the threshold contributions represented by the electric and magnetic polarizabilities, α_π and β_π, leading to the result

$$A(s,t) = 1 + \frac{\alpha_\pi + \beta_\pi}{4m_\pi \alpha}\left(s - m_\pi^2\right)\left(u - m_\pi^2\right), \tag{7}$$

$$B(s,t) = \frac{2m_\pi \beta_\pi}{\alpha}, \tag{8}$$

with α the fine-structure constant. In chiral-Lagrangian theory [3] numerical values are $\alpha_\pi + \beta_\pi = 0$ and $\alpha_\pi = 2.7 \times 10^{-4}$ fm^3.

A model for the energy dependence of the Compton amplitude can be obtained by invoking, in addition to the Born terms, the contributions from the $\sigma(0^+)$, $\rho(1^-)$, and $a_1(1^+)$ exchanges graphed in Fig. 2. Such models have been investigated in connection with studies of the reaction $\gamma\gamma \to \pi\pi$, and its t-channel counterpart $\gamma\pi \to \gamma\pi$. Numerical values of the model parameters have been extracted from experimental data by Fil'kov and Kashevarov [7].

The evaluation of the diagrams of Fig. 2 is straightforward. We parametrize the Compton amplitude through dimensionless functions $\lambda_1(s,t)$ and $\lambda_2(s,t)$ rather than $\alpha_\pi + \beta_\pi$ and β_π. Thus we introduce for the invariant functions $A(s,t)$ and $B(s,t)$ of Eq. (1) the decompositions

$$A(s,t) = 1 + \frac{\left(s - m_\pi^2\right)\left(u - m_\pi^2\right)}{4m_\pi^4}\lambda_1(s,t), \tag{9}$$

$$B(s,t) = \frac{2}{m_\pi^2}\lambda_2(s,t), \tag{10}$$

with the generalized polarizability functions as

$$\lambda_1(s,t) = -\frac{m_\pi^4}{2}\left\{g^2_{\rho\to\pi\gamma}\left(\frac{1}{s - m_\rho^2} + \frac{1}{u - m_\rho^2}\right) + g^2_{a_1\to\pi\gamma}\left(\frac{1}{s - m_{a_1}^2} + \frac{1}{u - m_{a_1}^2}\right)\right\}, \tag{11}$$

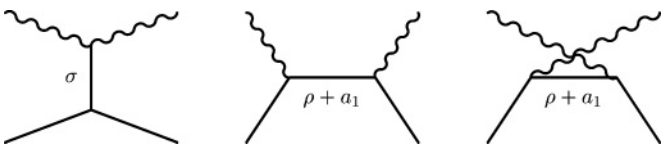

FIG. 2. Feynman diagrams for the σ, ρ, and a_1 contributions to pion-Compton scattering.

$$\lambda_2(s,t) = m_\pi^2\left\{g_{\sigma\to\pi\pi}\, g_{\sigma\to\gamma\gamma}\frac{1}{t - m_\sigma^2} - \frac{1}{4}g^2_{\rho\to\pi\gamma}\left(\frac{s + m_\pi^2}{s - m_\rho^2} + \frac{u + m_\pi^2}{u - m_\rho^2}\right) + \frac{1}{4}g^2_{a_1\to\pi\gamma}\left(\frac{s - m_\pi^2}{s - m_{a_1}^2} + \frac{u - m_\pi^2}{u - m_{a_1}^2}\right)\right\}. \tag{12}$$

At the pion-Compton threshold $s = u = m_\pi^2$ and $t = 0$. In chiral-Lagrangian theory the threshold values of the polarizability functions are $\lambda_1(m_\pi^2, 0) = 0$ and $\lambda_2(m_\pi^2, 0) = -0.013$. In the exchange model the threshold functions are dominated by σ exchange. However, the parameters of the σ are rather uncertain and we choose to fix them so that the σ contribution to the polarizability functions is twice as large as the chiral-Lagrangian prediction, and more in agreement with experiment [4,5]. This is further discussed in the Appendix. Thus, the σ-, ρ-, and a_1-exchange contributions to our threshold polarizability functions are

$$\lambda_1(s,t) = 0 + 0.0003 + 0.0003, \tag{13}$$

$$\lambda_2(s,t) = -0.0261 + 0.0004 + 0. \tag{14}$$

III. NUCLEAR CROSS SECTIONS

We are interested in a kinematic region where the transverse momentum components of particles can be neglected compared with their longitudinal momentum components. Details of the kinematics are given in [6]. The cross-section distribution in the pion-nucleus laboratory system is

$$\mathrm{d}\sigma = \frac{1}{4p_1 M_A}|\mathcal{M}|^2\,\mathrm{dLips}, \tag{15}$$

where p_1 is the incident pion laboratory momentum. The Lorentz-invariant phase space can be parametrized as

$$\mathrm{dLips} = \frac{1}{16\pi M_A}\frac{\mathrm{d}^2 p_{2\perp}}{(2\pi)^2}\frac{\mathrm{d}^2 q_{2\perp}}{(2\pi)^2}\frac{\mathrm{d}q_{2z}}{p_{2z}q_{2z}}. \tag{16}$$

The nuclear Born approximation is represented by the one-photon exchange graph as pictured in Fig. 3. The small blob in the graph represents the full pion-Compton amplitude; the large blob the photon-nucleus electromagnetic vertex. The pion charge is $-e$, the nuclear charge Ze, and the nucleus is treated as a spin-zero particle. With q_1 the virtual photon four-momentum, these assumptions lead to a Coulomb

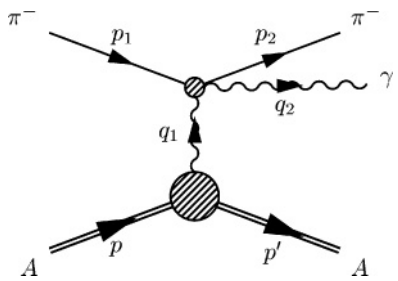

FIG. 3. Born diagram for pionic bremsstrahlung.

production amplitude

$$\mathcal{M}_B = \frac{-i}{q_1^2}\mathcal{M}_{\mu\nu}(p_2, q_2; p_1, q_1)(-iZe)(p+p')^\mu \epsilon_2^\nu. \quad (17)$$

Since the Compton tensor $\mathcal{M}_{\mu\nu}$ is gauge invariant we may also make the replacement $p + p' = 2p + q_1 \to 2p$.

The reduction of $\mathcal{M}_B$ is much simplified if we first introduce the parameter

$$x = \frac{q_{2z}}{p_1} = \frac{\omega_2}{E_1}. \quad (18)$$

Inserting in Eq. (17) the expansion of the pion-Compton amplitude from Eq. (1) and exploiting the techniques of [6] we get

$$\mathcal{M}_B = \frac{-8\pi i Z M_A e\alpha}{q_1^2}\left[4E_2 A(s,t)\left\{\frac{\mathbf{q}_{2\perp}}{\mathbf{q}_{2\perp}^2 + x^2 m_\pi^2} - \frac{\mathbf{q}_{2\perp} - x\mathbf{q}_{1\perp}}{(\mathbf{q}_{2\perp} - x\mathbf{q}_{1\perp})^2 + x^2 m_\pi^2}\right\} + \omega_2 B(s,t)\mathbf{q}_{1\perp}\right]\cdot\boldsymbol{\epsilon}_2. \quad (19)$$

The subscript $\perp$ indicates a vector component in the impact plane, i.e., the plane orthogonal to the incident momentum $\mathbf{p}_1$, which is along the z-direction. Note that the polarization vector $\boldsymbol{\epsilon}_2$ is orthogonal to $\mathbf{q}_2$, and therefore has both transverse and longitudinal components, the dominant one being transverse. Since $\mathbf{p}_{1\perp} = 0$ the transverse vector components are related by

$$\mathbf{q}_{1\perp} = \mathbf{p}_{2\perp} + \mathbf{q}_{2\perp}. \quad (20)$$

The second term on the right hand side of Eq. (19) has been slightly rewritten as compared with the corresponding term in Eq. (49) of [6]. As a consequence we see directly that the matrix element is proportional to $\mathbf{q}_{1\perp}$, as it should be.

We are interested in hard photons. Therefore, the parameter x of Eq. (18) is sizable, but still in the region $0 < x < 1$. We are also limiting ourselves to the Coulomb region, where $q_{1\perp}$ is of the same size as q_{1z}, which is equal to

$$q_{\min} = \frac{m_\pi^2\omega_2}{2E_1E_2} = xm_\pi(m_\pi/2E_2), \quad (21)$$

so that $q_{1\perp} \ll xm_\pi$. The momentum components $\mathbf{p}_{2\perp}$ and $\mathbf{q}_{2\perp}$, on the other hand, may both be in the GeV region but only in such a way that their sum $\mathbf{q}_{1\perp}$ remains the size of $q_{\min}$. It follows that

$$|x\mathbf{q}_{2\perp}\cdot\mathbf{q}_{1\perp}| \ll \left(\mathbf{q}_{2\perp}^2 + x^2m_\pi^2\right). \quad (22)$$

Application of this inequality simplifies the Born amplitude into

$$\mathcal{M}_B = \frac{-8\pi i Z M_A e\alpha}{q_1^2}\frac{4xE_2}{\mathbf{q}_{2\perp}^2 + x^2m_\pi^2}\left[\tilde{A}\left(x, \mathbf{q}_{2\perp}^2\right)\left\{\mathbf{q}_{1\perp} - 2\mathbf{q}_{2\perp}\frac{\mathbf{q}_{2\perp}\cdot\mathbf{q}_{1\perp}}{\mathbf{q}_{2\perp}^2 + x^2m_\pi^2}\right\} + \tilde{B}\left(x, \mathbf{q}_{2\perp}^2\right)\mathbf{q}_{1\perp}\right]\cdot\boldsymbol{\epsilon}_2, \quad (23)$$

with

$$\tilde{A}\left(x, \mathbf{q}_{2\perp}^2\right) = A(s,t), \quad (24)$$

$$\tilde{B}\left(x, \mathbf{q}_{2\perp}^2\right) = \frac{1}{4(1-x)}\left(\mathbf{q}_{2\perp}^2 + x^2m_\pi^2\right)B(s,t). \quad (25)$$

Here, we have replaced the variables s and t by the variables x and $\mathbf{q}_{2\perp}^2$. That this is possible follows from a study of the kinematic variables s, t, and u of the virtual pion-Compton scattering, defined in Eq. (4). Evaluating them with the on-shell four-momenta p_1, p_2, and q_2, and making use of the inequality (22) leads to the simple expressions

$$s - m_\pi^2 = \frac{1}{x(1-x)}\left[\mathbf{q}_{2\perp}^2 + x^2m_\pi^2\right],$$

$$t = \frac{-1}{1-x}\left[\mathbf{q}_{2\perp}^2 + x^2m_\pi^2\right], \quad (26)$$

$$u - m_\pi^2 = \frac{-1}{x}\left[\mathbf{q}_{2\perp}^2 + x^2m_\pi^2\right].$$

We stress that these expressions are valid only for hard bremsstrahlung in the Coulomb region. Furthermore, we may on the right hand sides replace $q_{2\perp}^2$ by $p_{2\perp}^2$ without any numerical consequences.

Up to now we have been concerned with the Born approximation, i.e., the one-photon exchange. Including multiple-photon exchanges to all orders induces some changes. The sole effect of photon exchanges that occur either all before or all after the hard-photon radiation is to dress the Born approximation with a Coulomb phase factor. Contributions where some photon exchanges occur before and some after the hard-photon radiation do not exhibit any peak structure, and are small in the Coulomb-peak region. This is also the case for radiation contributions involving hadronic interactions, which lead to a smooth background distribution much below the Coulomb peak, at least in the applications we have in mind. Adopting these caveats we put

$$|\mathcal{M}|^2 = \left|\mathcal{M}_B^2\right|. \quad (27)$$

The summation over the photon polarization vectors is trivial. It replaces scalar products like $|\mathbf{q}_{2\perp}\cdot\epsilon_2|^2$ by $|\mathbf{q}_{2\perp}|^2$. In view of the relation (20) we may also replace the phase-space volume $\mathrm{d}^2q_{2\perp}\mathrm{d}^2p_{2\perp}$ by $\mathrm{d}^2q_{1\perp}\mathrm{d}^2q_{2\perp}$. The cross-section distribution in the pion-nucleus laboratory system, as defined in Eq. (15), then takes the form

$$\frac{\mathrm{d}\sigma}{\mathrm{d}^2q_{1\perp}\mathrm{d}^2q_{2\perp}\mathrm{d}x} = \frac{4Z^2\alpha^3}{\pi^2m_\pi^4}\left[\frac{\boldsymbol{q}_{1\perp}^2}{\left(\boldsymbol{q}_{1\perp}^2 + q_{\min}^2\right)^2}\right]\left[\frac{1-x}{x^3}\right] \times\left[\left(\frac{x^2m_\pi^2}{\mathbf{q}_{2\perp}^2 + x^2m_\pi^2}\right)^2\right]\cdot\left|\tilde{A}\left(x, \mathbf{q}_{2\perp}^2\right)\times\left(\hat{\mathbf{q}}_{1\perp} - 2\mathbf{q}_{2\perp}\frac{\mathbf{q}_{2\perp}\cdot\hat{\mathbf{q}}_{1\perp}}{\mathbf{q}_{2\perp}^2 + x^2m_\pi^2}\right) + \tilde{B}\left(x, \mathbf{q}_{2\perp}^2\right)\hat{\mathbf{q}}_{1\perp}\right|^2. \quad (28)$$

The scalar functions $\tilde{A}(x, \mathbf{q}_{2\perp}^2)$ and $\tilde{B}(x, \mathbf{q}_{2\perp}^2)$ are defined in Eqs. (24) and (25). Introducing the functions $\lambda_1(x, \mathbf{q}_{2\perp}^2)$ and

$\lambda_2(x, \mathbf{q}_{2\perp}^2)$ of Eqs. (11) and (12) that describe the non-Born contributions we get

$$\tilde{A}\left(x, \mathbf{q}_{2\perp}^2\right) = 1 - \frac{x^2}{4(1-x)}\left(\frac{\mathbf{q}_{2\perp}^2 + x^2 m_\pi^2}{x^2 m_\pi^2}\right)^2 \lambda_1\left(x, \mathbf{q}_{2\perp}^2\right), \tag{29}$$

$$\tilde{B}\left(x, \mathbf{q}_{2\perp}^2\right) = \frac{x^2}{2(1-x)}\left(\frac{\mathbf{q}_{2\perp}^2 + x^2 m_\pi^2}{x^2 m_\pi^2}\right)\lambda_2\left(x, \mathbf{q}_{2\perp}^2\right). \tag{30}$$

The approximations leading to the cross-section distributions described by Eqs. (28)–(30) demand that the pionic radiation is hard, that the transverse components of the vectors $\mathbf{q}_2$ and $\mathbf{p}_2$ are much smaller than their longitudinal components, and that we are in the Coulomb dominated region where the length of the vector $\mathbf{q}_{1\perp} = \mathbf{p}_{2\perp} + \mathbf{q}_{2\perp}$ is of a size similar to that of $q_{1z} = q_{\min}$.

It is important to realise that although the cross-section distribution in general depends on the angle

$$\mu = \hat{\mathbf{q}}_{1\perp} \cdot \hat{\mathbf{q}}_{2\perp} = \cos\varphi_{12}, \tag{31}$$

the arguments of the polarizability functions λ_1 and λ_2 do not.

We end by reemphasizing that s, t, and u are variables of the virtual pion-Compton scattering. The momentum transfer squared to the nucleus is

$$-t_A = \mathbf{q}_{1\perp}^2 + q_{\min}^2. \tag{32}$$

IV. UNDER THE COULOMB PEAK: I

Results concerning the pion polarizabilities are most easily discussed for the phase-space region where the transverse momentum $q_{2\perp}$ is small, to be more precise,

$$\mathbf{q}_{2\perp}^2 \ll x^2 m_\pi^2. \tag{33}$$

The same restriction then applies to $\mathbf{p}_{2\perp}^2$, since in the Coulomb region the size of their vector sum $q_{1\perp} = |\mathbf{q}_{2\perp} + \mathbf{p}_{2\perp}|$ must be of the order of $q_{\min}$, and since we deduce from Eq. (21) that the ratio $q_{\min}/x m_\pi = m_\pi/2E_2$ must be utterly small. In this kinematical situation the variables s, t, and u of the pion-Compton amplitude, Eq. (26), become simple functions of x

$$\begin{aligned} s &= m_\pi^2/(1-x), \\ t &= -x^2 m_\pi^2/(1-x), \\ u &= (1-x)m_\pi^2. \end{aligned} \tag{34}$$

The cross section can be written as

$$\begin{aligned} &\frac{\mathrm{d}\sigma}{\mathrm{d}^2 q_{1\perp}\mathrm{d}^2 q_{2\perp}\mathrm{d}x} \\ &\quad = \frac{4Z^2\alpha^3}{\pi^2 m_\pi^4}\left[\frac{\boldsymbol{q}_{1\perp}^2}{\left(\boldsymbol{q}_{1\perp}^2 + q_{\min}^2\right)^2}\right]\left[\frac{1-x}{x^3}\right] \cdot \\ &\qquad \times \left|1 + \frac{x^2}{1-x}\left(-\frac{1}{4}\lambda_1(x) + \frac{1}{2}\lambda_2(x)\right)\right|^2, \end{aligned} \tag{35}$$

with $x = \omega_2/E_1$ from Eq. (18). We conclude that in general the contributions from the pion structure terms are small. Only if x is very near unity do we get a substantial contribution. This means bremsstrahlung photons of energies very near those of the incident pion. We also observe that when $x \approx 1$ the energy in the pion-Compton scattering may become so large that the threshold approximation to the polarizability functions breaks down.

Our model expression for the combination of polarizability functions encountered in Eq. (35) is

$$\begin{aligned} &-\frac{1}{4}\lambda_1(x) + \frac{1}{2}\lambda_2(x) \\ &\quad = -\frac{1}{2} g_{\sigma\to\pi\pi} g_{\sigma\to\gamma\gamma} \frac{1-x}{x^2 + \hat{m}_\sigma^2(1-x)} - \frac{1}{8} m_\pi^2 g_{\rho\to\pi\gamma}^2 \\ &\qquad \times \left[\frac{1}{1 - \left(\hat{m}_\rho^2 - i\hat{m}_\rho\hat{\Gamma}_\rho(x)\right)(1-x)} + \frac{1}{1 - \hat{m}_\rho^2/(1-x)}\right] \\ &\qquad + \frac{1}{8} m_\pi^2 g_{a_1\to\pi\gamma}^2 \left[\frac{1}{1 - \left(\hat{m}_{a_1}^2 - i\hat{m}_{a_1}\hat{\Gamma}_{a_1}(x)\right)(1-x)}\right. \\ &\qquad \left. + \frac{1}{1 - \hat{m}_{a_1}^2/(1-x)}\right], \end{aligned} \tag{36}$$

with masses and widths normalized to the pion mass, $\hat{m} = m/m_\pi$ and $\hat{\Gamma} = \Gamma/m_\pi$. Remember that resonance widths are non-vanishing only if the pion-Compton c.m. energy $s(x)$ is above the threshold energy for resonance decay.

We illustrate the sensitivity to the polarizability functions and their energy dependence by plotting in Fig. 4 the proportionality function

$$R(x, \lambda(x)) = \left|1 + \frac{x^2}{1-x}\left(-\frac{1}{4}\lambda_1(x) + \frac{1}{2}\lambda_2(x)\right)\right|^2, \tag{37}$$

together with $R(x, \lambda(0))$. The curves are plotted for x in the interval (0.6, 0.97) and the input parameters are those of the exchange model of Sec. II. It is feasible to extract information about the polarizability functions only if $R(x, \lambda(x))$ deviates appreciably from unity, which occurs when x approaches one. When this happens the curves for $R(x, \lambda(x))$ and $R(x, \lambda(0))$ start to diverge from each other. Thus, when the polarizability

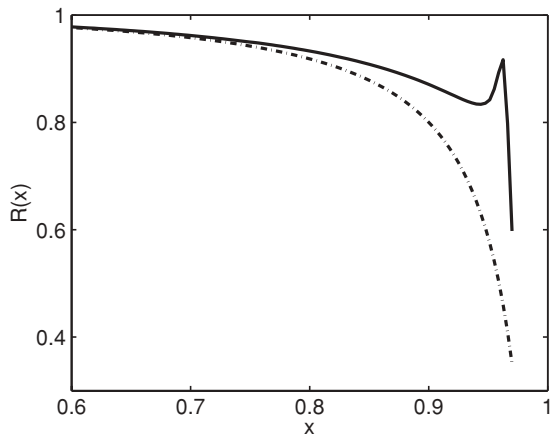

FIG. 4. Proportionality function $R(x)$ in the Coulomb region, at momentum transfers $q_{2\perp}^2$, $p_{2\perp}^2 \ll x^2 m_\pi^2$. The solid line obtains in the full calculation, the dash-dotted line in the threshold approximation.

contributions become appreciable the threshold approximation deteriorates. The structure in the solid curve at $x \approx 0.96$, corresponding to $\sqrt{s} \approx m_\rho$, is caused by the ρ-meson contribution to the pion-Compton amplitude.

V. UNDER THE COULOMB PEAK: II

Our investigation presumes two conditions; the transverse components of the vectors $\mathbf{p}_2$ and $\mathbf{q}_2$ must be much smaller than their longitudinal components, and their sum $\mathbf{p}_{2\perp} + \mathbf{q}_{2\perp} = \mathbf{q}_{1\perp}$ must be in the Coulomb region, i.e., in the region where the length of $\mathbf{q}_{1\perp}$ is of a size similar to $q_{\min}$. If these conditions are not met, we are outside the Coulomb peak and nuclear contributions play a role. Even though the sum of the two vector components $\mathbf{p}_{2\perp}$ and $\mathbf{q}_{2\perp}$ must be very small, this need not be so for the two vector components individually. We shall now consider the case where they are large, meaning large in comparison with m_π.

The general expression for the cross-section distribution, Eq. (28), can be rewritten as

$$\begin{aligned}\frac{\mathrm{d}\sigma}{\mathrm{d}^2q_{1\perp}\mathrm{d}^2q_{2\perp}\mathrm{d}x} &= \frac{4Z^2\alpha^3}{\pi^2 m_\pi^4}\left[\frac{\boldsymbol{q}_{1\perp}^2}{\left(\boldsymbol{q}_{1\perp}^2+q_{\min}^2\right)^2}\right]\left[\frac{1-x}{x^3}\right]\\ &\times\left[\left(\frac{x^2m_\pi^2}{\mathbf{q}_{2\perp}^2+x^2m_\pi^2}\right)^2\right]\cdot\Big[\left|\tilde{A}\left(x,\mathbf{q}_{2\perp}^2\right)\right|^2\left\{1-\mu^2\right.\\ &\times\left.\left(1-\kappa^2\right)\right\}+2\Re\left(\tilde{A}\left(x,\mathbf{q}_{2\perp}^2\right)\tilde{B}^*\left(x,\mathbf{q}_{2\perp}^2\right)\right)\left\{1-\mu^2\right.\\ &\times\left.(1-\kappa)\right\}+\left|\tilde{B}\left(x,\mathbf{q}_{2\perp}^2\right)\right|^2\Big],\end{aligned} \tag{38}$$

with κ defined as

$$\kappa\left(x,\mathbf{q}_{2\perp}^2\right)=\frac{x^2m_\pi^2-\mathbf{q}_{2\perp}^2}{x^2m_\pi^2+\mathbf{q}_{2\perp}^2}. \tag{39}$$

A simple angular dependence enters through the variable $\mu = \hat{\mathbf{q}}_{1\perp}\cdot\hat{\mathbf{q}}_{2\perp}$ and an average over angles replaces μ^2 by its average of one half.

In Sec. IV we studied the small momentum transfer region where $\mathbf{q}_{2\perp}^2 \ll x^2m_\pi^2$. As this implies $\kappa \approx 1$ the angular dependent terms in Eq. (38) drop out. Also, the right hand side of this equation was found to be independent of $\mathbf{q}_{2\perp}^2$, leaving only a dependence on x, and the characteristic Coulomb-peak prefactor depending on $\mathbf{q}_{1\perp}^2$.

Now, we turn to the region of large transverse momenta, i.e., momenta such that

$$\mathbf{q}_{2\perp}^2 \gg x^2m_\pi^2. \tag{40}$$

As explained at the beginning of this section, this implies that, under the Coulomb peak, $\mathbf{p}_{2\perp}^2 \gg x^2m_\pi^2$ as well. The expressions for the kinematic variables in the Compton process then simplify somewhat, replacing Eq. (26) by

$$\begin{aligned}s &= m_\pi^2+\frac{\mathbf{q}_{2\perp}^2}{x(1-x)},\\ t &= -\frac{\mathbf{q}_{2\perp}^2}{1-x},\\ u &= m_\pi^2-\frac{\mathbf{q}_{2\perp}^2}{x}.\end{aligned} \tag{41}$$

At large tranverse momenta, it follows from the definition of κ, Eq. (39), that $\kappa \approx -1$. As a consequence, in the cross-section distribution of Eq. (38), the angular dependence in the term proportional to $|\tilde{A}|^2$ drops out, and after integration over angles the cross term proportional to $\Re(\tilde{A}\tilde{B}^*)$ vanishes. Since the term proportional to $|\tilde{B}|^2$ carries no angular dependence an average over angles leads to the cross-section distribution

$$\begin{aligned}\frac{\mathrm{d}\sigma}{\mathrm{d}q_{1\perp}^2\mathrm{d}q_{2\perp}^2\mathrm{d}x} &= \frac{4Z^2\alpha^3}{\boldsymbol{q}_{2\perp}^4}\left[\frac{\boldsymbol{q}_{1\perp}^2}{\left(\boldsymbol{q}_{1\perp}^2+q_{\min}^2\right)^2}\right]x(1-x)\\ &\cdot\left[\left|\tilde{A}\left(x,\mathbf{q}_{2\perp}^2\right)\right|^2+\left|\tilde{B}\left(x,\mathbf{q}_{2\perp}^2\right)\right|^2\right].\end{aligned} \tag{42}$$

The invariant functions entering this equation are defined in Eqs. (24) and (25) and Eqs. (7) and (8), and read

$$\tilde{A}\left(x,\mathbf{q}_{2\perp}^2\right)=1-\frac{1}{4x^2(1-x)}\left(\frac{\mathbf{q}_{2\perp}^2}{m_\pi^2}\right)^2\lambda_1\left(x,\mathbf{q}_{2\perp}^2\right), \tag{43}$$

$$\tilde{B}\left(x,\mathbf{q}_{2\perp}^2\right)=\frac{1}{2(1-x)}\left(\frac{\mathbf{q}_{2\perp}^2}{m_\pi^2}\right)\lambda_2\left(x,\mathbf{q}_{2\perp}^2\right). \tag{44}$$

We notice that the polarizability contributions to the functions $\tilde{A}$ and $\tilde{B}$ are enhanced by powers of the factor $\mathbf{q}_{2\perp}^2/m_\pi^2$.

Finally, in the phase-space element of the cross-section distribution (42) we may introduce the momentum transfer to the nucleus t_A via the identity

$$\mathrm{d}q_{1\perp}^2 = -\mathrm{d}t_A. \tag{45}$$

We illustrate the sensitivity of the cross-section distributions to the polarizability functions and their energy dependence in the same way as we did for small transverse momenta in Sec. IV. Thus, introduce the proportionality function

$$R\left(x,\mathbf{q}_{2\perp}^2;\lambda\left(x,\mathbf{q}_{2\perp}^2\right)\right)=\left|\tilde{A}\left(x,\mathbf{q}_{2\perp}^2\right)\right|^2+\left|\tilde{B}\left(x,\mathbf{q}_{2\perp}^2\right)\right|^2 \tag{46}$$

which now depends on both x and $\mathbf{q}_{2\perp}^2$. Putting λ_1 and λ_2 equal to zero leads to $R = 1$, the value for a point-like pion.

In Fig. 5 we graph the proportionality function $R(x,\mathbf{q}_{2\perp}^2;\lambda(x,\mathbf{q}_{2\perp}^2))$ and the function $R(x,\mathbf{q}_{2\perp}^2;\lambda(0))$, which is the same function but evaluated with the threshold values of the polarizabilities. For the illustration we have chosen $q_{2\perp} = 3.5m_\pi$. From Eq. (41) it then follows that $s \geqslant 50m_\pi^2$ and far from its threshold value $s = m_\pi^2$. The curves are plotted for x in the region $0.2 \leqslant x \leqslant 0.8$, corresponding to $\sqrt{s}$ in the region $990 \leqslant \sqrt{s} \leqslant 1230$, in units of MeV. In view of the large energies it is not astonishing to note that the threshold approximation is unrealistic. The solid curve which represents the full calculation is not symmetric around $x = 0.5$ even though the energy s is. The reason is that neither t nor u is symmetric. Therefore, the cross sections at $x = 0.4$ and $x = 0.6$, e.g., measure pion-Compton cross-sections at the same energy but at completely different scattering angles.

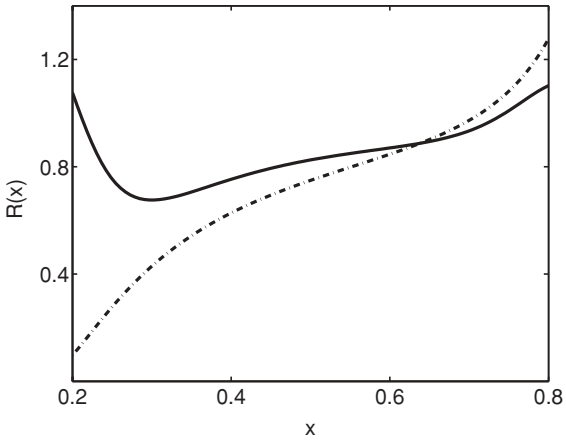

FIG. 5. Proportionality function $R(x, \mathbf{q}_{2\perp}^2; \lambda(x, \mathbf{q}_{2\perp}^2))$ for $q_{2\perp} = p_{2\perp} = 3.5m_\pi$ in the Coulomb region. The solid line obtains in the full calculation, the dash-dotted line in the threshold approximation.

However, since the cross-section distribution displayed in Fig. 5 is markedly different from the corresponding distribution for point-like pions, $R = 1$, hard pionic bremsstrahlung should be a good place for probing models for pion-Compton scattering.

VI. SUMMARY

Hard bremsstrahlung in high-energy pion-nucleus scattering in the Coloumb region has been investigated. The kinematics of the reaction can be read off from

$$\pi^-(p_1) + A(p) \to \gamma(q_2) + \pi^-(p_2) + A(p').$$

The restriction to the Coulomb region means that the momentum transfer to the nucleus is of the order of $q_{\min} = m_\pi^2\omega_2/(2E_1E_2)$. As a consequence, the production amplitude is dominated by the one-photon exchange diagram and the cross-section distribution exhibits the well-known Coloumb-production peak structure. In the Coloumb region the sum of the transverse momenta

$$\mathbf{p}_{2\perp} + \mathbf{q}_{2\perp} = \mathbf{q}_{1\perp},$$

is tiny, although the transverse momenta themselves need not be that small.

We have derived an expression for the cross-section distribution, Eq. (38), valid when the transverse momenta of the emerging photon and pion are much smaller than their longitudinal momenta. The arguments of this expression are $x = \omega_2/E_1$ and $\mathbf{q}_{2\perp}^2$, which for all practical purposes is the same as $\mathbf{p}_{2\perp}^2$. The nuclear production amplitude involves the on-shell pion-Compton amplitude at energies and angles that depend on the values of x and $\mathbf{q}_{2\perp}^2$, Eq. (26). The pion-Compton amplitude is modelled as a sum of the point-like Born terms and the polarizability terms, represented by σ, ρ, and a_1 exchange-diagram terms.

We have illustrated our model by considering two limits; in the first one, the limit of small transverse momenta, the sizes of both $|\mathbf{q}_{2\perp}|$ and $|\mathbf{p}_{2\perp}|$ are much smaller than m_π, whereas in the second one, the limit of large transverse momenta, their sizes are both much larger than m_π, but in such a way that their vector sum remains tiny.

In the region of small transverse momenta the pion-Compton amplitude depends only on x. When x is small the influence of the polarizability functions on the bremsstrahlung cross section is weak. In order to be noticed we must go to x-values near unity. Then, the energy at which the pion-Compton amplitude is evaluated becomes so large that the threshold approximation of the polarizability functions becomes questionable. To extract reliable values for the famous coefficients α_π and β_π requires accurate experiments.

In the region of large transverse momenta the effective energies in the pion-Compton amplitudes are several times larger than the pion mass and the threshold approximation to the polarizability functions not applicable. Moreover, the polarizability functions develop imaginary parts that are important. We have also stressed that the nuclear cross-section distribution is not related in a simple way to a pion-Compton cross section at a fixed energy, since the energy s and momentum transfer t in the pion-Compton scattering are functions of x and $\mathbf{q}_{2\perp}^2$. However, the bremsstrahlung cross section strongly depends on the pion-Compton amlitude and thus offers a good opportunity to check models for this amplitude.

A bremsstrahlung experiment with pions of 40 GeV/c was undertaken some years ago [4]. The cross-section distribution was measured in the Coulomb region and the pion polarizabilities were extracted in the equivalent photon approximation. The sum $\alpha_\pi + \beta_\pi$ was found to be consistent with zero, in accordance with predictions of chiral-Lagrangian theory. Furthermore, it was found that $\alpha_\pi = (6.8 \pm 1.4) \times 10^{-4}$ fm^3, about twice as large as predicted. A new, similar, experiment has been performed by the COMPASS collaboration at CERN. Their results are at the moment being analyzed.

ACKNOWLEDGMENTS

We would like to thank Jan Friedrich and Andrej Arbuzov of the COMPASS collaboration for very informative discussions.

APPENDIX

In this appendix the parameters of the pion-Compton model are discussed.

The radiative decay of the sigma meson has width and coupling constant related by

$$\Gamma(\sigma \to \gamma\gamma) = \pi\alpha^2 g_{\sigma\to\gamma\gamma}^2 m_\sigma^3. \quad \text{(A1)}$$

For the strong decay of the sigma meson the corresponding relation is

$$\Gamma(\sigma \to \pi^+\pi^-) = \frac{1}{16\pi m_\sigma} g_{\sigma\to\pi\pi}^2 \sqrt{1 - \frac{4m_\pi^2}{m_\sigma^2}}. \quad \text{(A2)}$$

Numerical values for the coupling constants have been extracted by Fil'kov and Kashevarov [7] from a study of data for the reaction $\gamma\gamma \to \pi^0\pi^0$. Their results are $\Gamma(\sigma \to \gamma\gamma) = 0.62$ keV, $\Gamma(\sigma \to \pi^+\pi^-) = 803$ MeV, and $m_\sigma = 547$ MeV.

For the product of coupling constants these numbers give $g_{\sigma\to\gamma\gamma}g_{\sigma\to\pi\pi} = 0.762$, which results in a value for β_{π^+} almost four times as large as the chiral-Lagrangian prediction. In view of the uncertainty of the σ parameters we shall choose

$$g_{\sigma\to\gamma\gamma}g_{\sigma\to\pi\pi} = 0.400, \tag{A3}$$

giving a value more in line with experimental prejudices [4,5].

The s-channel propagators of the ρ and a_1 mesons are given Breit-Wigner shapes

$$B^L(s) = \frac{m_0^2}{\left(m_0^2 - s\right) - im_0\Gamma^L(s)}, \tag{A4}$$

$$\Gamma^L(s) = \Gamma_0\left(\frac{k}{k_0}\right)^{2L+1}\frac{m_0}{\sqrt{s}}\theta\left(\sqrt{s} - m_1 - m_2\right), \tag{A5}$$

where Γ_0 and m_0 are nominal values and k_0 the decay momentum at mass m_0. The momentum is

$$k(s) = \frac{1}{2m_0}[(s - (m_1 + m_2)^2)(s - (m_1 - m_2)^2)]^{1/2}. \tag{A6}$$

Furthermore, $L = 1$ for $\rho \to \pi\pi$ whereas $L = 0$ for $a_1 \to \rho\pi$. The total nominal widths are $\Gamma_\rho = 150$ MeV, $\Gamma_{a_1} = 450$ MeV, and the masses are $m_\pi = 139.6$ MeV, $m_\rho = 775$ MeV, $m_{a_1} = 1230$ MeV.

The relations between width and coupling constant for the ρ meson is

$$\Gamma(\rho^+ \to \pi^+\gamma) = \tfrac{1}{3}\alpha g^2_{\rho\to\pi\gamma}\left[\frac{m_\rho^2 - m_\pi^2}{2m_\rho}\right]^3. \tag{A7}$$

With a numerical value for the width $\Gamma(\rho^+ \to \pi^+\gamma) = 68$ keV the coupling constant becomes

$$m_\rho g_{\rho\to\pi\gamma} = 0.5644. \tag{A8}$$

The relations between width and coupling constant for the a_1 meson is

$$\Gamma(a_1^+ \to \pi^+\gamma) = \tfrac{1}{3}\alpha g^2_{a_1\to\pi\gamma}\left[\frac{m_{a_1}^2 - m_\pi^2}{2m_{a_1}}\right]^3. \tag{A9}$$

This relation is exactly the same as the one for the ρ meson even though the parities of the ρ and a_1 mesons differ. With a numerical value for the width $\Gamma(a_1^+ \to \pi^+\gamma) = 640$ keV the coupling constant becomes

$$m_{a_1} g_{a_1\to\pi\gamma} = 1.334. \tag{A10}$$

[1] A. Halprin, C. M. Andersen, and H. Primakoff, Phys. Rev. **152**, 1295 (1966).

[2] A. S. Gal'perin *et al*., Sov. J. Nucl. Phys. **32**, 545 (1980).

[3] M. V. Terent'ev, Sov. J. Nucl. Phys. **16**, 87 (1973); J. Bijnens and F. Cornet, Nucl. Phys. **B296**, 557 (1988); J. F. Donoghue and B. R. Holstein, Phys. Rev. D **40**, 2378 (1989).

[4] Yu. M. Antipov *et al*., Phys. Lett. **B121**, 445 (1983); Yu. M. Antipov *et al*., Z. Phys. C **24**, 39 (1984); **26**, 495 (1984).

[5] J. Ahrens *et al*., Eur. Phys. J. A **23**, 113 (2005).

[6] G. Fäldt, Phys. Rev. C **76**, 014608 (2007).

[7] L. V. Fil'kov and V. L. Kashevarov, Eur. Phys. J. A **5**, 285 (1999).